



13 Abstract

14 Shallow groundwater in the Prairie Pothole Region (PPR) is recharged predominantly by snowmelt
15 in the spring and may supply water for evapotranspiration through the summer/fall. This two-way
16 exchange is underrepresented in land-surface models. Furthermore, the impacts of climate change
17 on the groundwater recharge are uncertain. In this paper, we use a coupled land and groundwater
18 model to investigate the hydrologic cycle of shallow groundwater in the PPR and study its response
19 to climate change at the end of the 21st century. The results show that the model reasonably
20 simulates the water table depth (WTD) and the timing of recharge processes, but underestimates
21 the seasonal variation of WTD, due to mismatches of the soil types between observations and the
22 model. The most significant change under future climate occurs in the winter, when warmer
23 temperature changes the rain/snow partitioning, delay the time for snow accumulation/soil
24 freezing while bring forward early melting/thawing. Such changes lead to an earlier start to a
25 longer recharge season, but with lower recharge rates. Different signals are shown in the eastern
26 and western PPR in the future summer, with reduced precipitation and drier soils in the east but
27 little change in the west. The annual recharge increased by 25% and 50% in the eastern and western
28 PPR, respectively. Additionally, we found the mean and seasonal variation of the simulated
29 WTD are sensitive to soil properties and fine-scale soil information is needed to improve
30 groundwater simulation on regional scale.

31

32 Keywords: Groundwater, Recharge, Climate Change, Prairie Pothole Region, Hydrologic Cycle,



33 Introduction

34 [1] Groundwater (GW) is an important source of freshwater for human beings. The domestic needs
35 of about half of the world's population (UNESCO, 2004) and 38% of the global water demand
36 for irrigation are provided by groundwater (Siebert et al., 2010). In the Canadian prairies, more
37 than 30% of the population relied on groundwater in 1996 (Statistics Canada, 1996). In a more
38 recent survey, while 90% of the municipal population is now provided by surface water sources,
39 more than 50% of the population living in rural areas are still relying on groundwater sources in
40 Canada (Environment Canada, 2011). In the U.S., up to 90% of water for drinking and irrigation
41 are provided by groundwater across different parts of the country (National Research Council,
42 2003).

43

44 [2] The groundwater flows in cold regions exhibit unique hydrological characteristics due to the
45 hydraulic isolation, induced by seasonally frozen soil (Ireson et al., 2013). As frozen soils reduce
46 permeability and snow accumulates during winter, the timing of groundwater recharge is
47 controlled by the snowmelt and soil thaw period in spring. Previous work by Kelln et al. (2007)
48 found that the timing of the recharge was associated strongly with soil thaw, rather than snowmelt,
49 and occurred one to six weeks later than snowmelt. On the other hand, previous observations in a
50 glacial-till site, where groundwater flow to underlying aquifer and lateral flow are small, have
51 suggested the decline of water table during winter is related to an upward water transport to the
52 freezing front (Remenda et al., 1996).

53

54 [3] The Prairie Pothole Region (PPR) in North America is located in a semi-arid and cold region,
55 where evapotranspiration (ET) exceeds precipitation (PR) in summer and near-surface soil is



56 frozen in winter (Gray, 1970; Granger and Gray, 1989; Hayashi et al., 2003; Pomeroy et al., 2007;
57 Ireson et al., 2013; Dumanski et al., 2015). The groundwater recharge to shallow aquifers in the
58 PPR is crucially influenced by these climatic conditions and seasonal freeze-thaw processes.
59 During the winter, snow accumulation and frozen near-surface soil prohibit infiltration. At the
60 same time, the water table slowly declines due to a combination of upward transport to freezing
61 front by the capillary effect and discharge to river (Ireson et al., 2013). In the early spring,
62 snowmelt becomes the dominant component of the hydrologic cycle and the melt water runs over
63 frozen soil, with little infiltration contributing to recharge. As the soil thaws, the increased
64 infiltration capacity allows snowmelt recharge reaching the water table, the previously upward
65 water movement by capillary effect move downwards, and water table rises to its maximum level.
66 In the summer and fall, when high ET exceeds PR and desiccates the soil, capillary rise may draw
67 water from the groundwater aquifers to supply ET demands, declining water table. This two-way
68 exchange between unsaturated soils and groundwater aquifers is important for the water table
69 dynamics on regional scale.

70

71 [4] Furthermore, groundwater exchange with prairie pothole wetlands are complicated and critical
72 in the PPR. Numerous wetlands known as potholes or sloughs provide important ecosystem
73 services, such as providing wildlife habitats and groundwater recharge (Johnson et al., 2010).
74 Shallow groundwater aquifers may receive water from or lose water to prairie wetlands depending
75 on the hydrological setting. Depression-focused recharge generated by runoff from upland to
76 depression contributes to sufficient amount of water input to shallow groundwater (5-40 mm/year).
77 On the other hand, groundwater lateral flow exchange center of a wetland pond to its moist margin
78 is also an important components in the wetland water balance (van der Kamp and Hayashi, 2009;



79 Brannen, et al., 2015; Hayashi et al., 2016). However, this groundwater-wetland exchange
80 typically occurs on local scale (from 10 to 100 m) and thus, challenging to in current land surface
81 models or climate models (resolution from 1 km to 100 km). Therefore, in this paper, we tend to
82 focus on the groundwater dynamics in PPR on regional scale two-way exchange between aquifer
83 and soils, rather than local scale groundwater-wetland exchange.

84

85 [5] Previous studies have suggest that substantial changes to groundwater interactions with above
86 soils are likely to occur under climate change (Tremblay et al., 2011; Green et al., 2011; Ireson et
87 al., 2013, 2015). Existing modeling studies on the impacts of climate change on groundwater are
88 either at global or basin/location-specific scales (Meixner et al., 2016). Global-level groundwater
89 studies focus on potential future recharge trends (Doll and Fiedler, 2008; Doll, 2009), yet coarse
90 resolution analysis from global climate models (GCMs) provided little specificity to inform
91 decision making. Basin-scale groundwater studies connect the climate with groundwater-flow
92 models to understand the climate impacts on specific systems (Maxwell and Kollet, 2008; Kurylyk
93 and MacQuarrie, 2013; Dumanski et al., 2015). However, a knowledge gap exists in predicting the
94 effect of climate change over large regions (major river basins, states or group of states) (Green et
95 al., 2011). The lack of climate-groundwater studies at regional scale may be due to two reasons:
96 first, it is challenging to represent the two-way water exchange in coupled land surface and
97 groundwater model at a regional scale; and second, a regional coupled land-hydrology model
98 requires fine-resolution and good quality meteorological forcing, which needs to be further
99 downscaled from GCMs.

100



101 [6] Recently, the two-way exchange has been implemented in coupled land surface – groundwater
102 models (LSM-GW), but is still challenging to apply to cold regions. For example, Maxwell and
103 Miller (2005) used a groundwater model (ParFlow) coupled with the Common Land Model (CLM).
104 They found that the coupled and uncoupled model is very similar in simulated sensible heat flux
105 (SH), ET, and shallow soil moisture (SM), but are different greatly in runoff and deep SM. This is
106 perhaps because only downwards flow from soil to groundwater is considered. Later on, Kollet
107 and Maxwell (2008) incorporated the ET effect on redistributing moisture upward from shallow
108 water table depth (WTD) and found the surface energy partition is highly sensitive to a WTD
109 ranging from 1 – 5 m. More recently, Niu et al. (2011) implemented a simple groundwater model
110 (SIMGM, Niu et al., 2007), into the community Noah LSM with multi-parameterization options
111 (Noah-MP LSM), by adding an unconfined aquifer at the bottom of soil layers. In order to
112 reasonably capture the groundwater regime in the PPR under semi-arid and seasonally frozen soil
113 climatic conditions, a coupled LSM-GW with the ability of addressing the two-way exchange
114 between soil and groundwater as well as representing the freeze-thaw process is necessary.

115

116 [7] In addition to representing the two-way water exchange, the spatial heterogeneity of soil
117 moisture and WTD requires meteorological forcing in high spatial resolution, that are not available
118 from direct output of coarse resolution GCMs. Furthermore, great uncertainties of simulated
119 precipitation stem from choice of convection parameterization schemes in GCMs (Sherwood et al.,
120 2014; Prein et al., 2015). For example, convective precipitation, an important source of
121 precipitation in the PPR in summer, its frequency, diurnal cycle and propagation are poorly
122 captured by GCM's parameterizations (Rasmussen et al., 2017). An important approach to
123 improve precipitation simulation is to use the convection-permitting model (CPM) (Ban et al.,



124 2014; Prein et al., 2015; Liu et al., 2017). The CPM uses a high spatial resolution in the atmosphere
125 (usually under 5-km) to explicitly resolve convection and not activate convection parameterization
126 schemes. On the other hand, CPMs can also improve the representation of fine-scale topography
127 and spatial variations of surface fields (Prein et al., 2013). These CPM added-values provide an
128 excellent opportunity to investigate groundwater evolution in the PPR.

129

130 [8] Therefore, the purpose of this paper is to investigate the hydrological changes in groundwater
131 in PPR under climate change and understand the drivers for different hydrological processes. Our
132 goal is to 1) simulate the two-way water exchange in the PPR using a coupled land-groundwater
133 model, 2) capture changes in the groundwater regime under climate change, and 3) identify major
134 climatic and land surface processes that contribute to these changes in the PPR. We use a
135 deterministic distributed physical process-based LSM (Noah-MP LSM) coupled with a
136 groundwater dynamics model, called the MMF model (developed by Fan et al. (2007) and Miguez-
137 Macho et al. (2007)). The coupled Noah-MP-MMF model is driven by two sets of meteorological
138 forcing for 13 years under current and future climate scenarios. These two sets of meteorological
139 dataset are from a CPM dynamical downscale project using the Weather Research & Forecast
140 (WRF) model with 4-km grid spacing in the Contiguous U.S. (WRF CONUS, Liu et al., 2017).

141

142 [9] The paper is structured as follow: Section 2 introduces the observational data for WTD in the
143 PPR, the coupled Noah-MP-MMF model, and the meteorological forcing from WRF CONUS
144 project. Section 3 evaluates the model simulated WTD timeseries against observations and shows
145 the groundwater budget and hydrological changes due to climate change. Section 4 and 5 offer a
146 broad discussion and conclusion to the paper.



147 2. Data and Methods

148 2.1 Observation data

149 [10] Groundwater observation data were obtained through several agencies: (1) the United States
150 Geological Survey (USGS) National Water Information System in the U.S.
151 ([https://waterdata.usgs.gov/nwis/uv?referred_module=gw&search_criteria=search_site_no&search](https://waterdata.usgs.gov/nwis/uv?referred_module=gw&search_criteria=search_site_no&search_criteria=site_tp_cd&submitted_form=introduction)
152 [ch_criteria=site_tp_cd&submitted_form=introduction](http://aep.alberta.ca/water/programs-and-services/groundwater/groundwater-observation-well-network/default.aspx)), (2) the Alberta Environment
153 ([http://aep.alberta.ca/water/programs-and-services/groundwater/groundwater-observation-well-](http://aep.alberta.ca/water/programs-and-services/groundwater/groundwater-observation-well-network/default.aspx)
154 [network/default.aspx](https://www.wsask.ca/Water-Info/Ground-Water/Observation-Wells/)), (3) the Saskatchewan Water Security Agency
155 (<https://www.wsask.ca/Water-Info/Ground-Water/Observation-Wells/>), and (4) the Manitoba
156 Water Stewardship Division
157 ([https://manitoba.maps.arcgis.com/apps/webappviewer/index.html?id=28fc1a53c9f8435d897501](https://manitoba.maps.arcgis.com/apps/webappviewer/index.html?id=28fc1a53c9f8435d897501724766a992)
158 [724766a992](https://manitoba.maps.arcgis.com/apps/webappviewer/index.html?id=28fc1a53c9f8435d897501724766a992)). Initially, groundwater data from 166 wells were acquired, 40 in US, 56 from Alberta,
159 61 from Saskatchewan, and nine from Manitoba.

160

161 [11] Despite the data acquired from a large number of wells, not all of the wells were suitable for
162 the study of shallow groundwater and climate change. We used the following criteria to select
163 qualified stations for our study and evaluate our model performance against these observations:

- 164 1) a sufficiently long record of groundwater measurement record during the simulation period;
- 165 2) minimal anthropogenic effects (such as pumping or irrigation);
- 166 3) unconfined aquifers with shallow groundwater levels (top 7 meters below surface).

167



168 These criteria reduced the observation data to the record of 11 well records, with one in Alberta,
169 six in Saskatchewan and four in Minnesota (U.S.). **Table 1** summarizes the information for each
170 selected well, and **Fig. 1(a)** shows the location of the wells in our study area.

171

172 **Fig. 1** (a) Topography of the Prairie Pothole Region (PPR) and station location of rain gauges (black dots) and
173 groundwater wells (red diamonds); (b) Topography of the WRF CONUS domain, with the black box indicating the
174 PPR domain.

175

176 **Table 1** Summary of the locations and aquifer type and soil type of the 11 selected wells.

177



178 2.2 Groundwater Scheme in Noah-MP

179 [12] In the present study, we used the community Noah-MP LSM (Niu et al. 2011; Yang et al.
 180 2011), coupled with a GW model – the MMF model, (Fan et al. 2007; Miguez-Macho et al., 2007).
 181 This coupled model has been applied in many regional hydrology studies in offline mode (Miguez-
 182 Macho and Fan 2012; Martinez et al., 2016) as well as coupled with regional climate models
 183 (Anyah et al., 2008; Barlage et al., 2015). We present here a brief introduction to the MMF
 184 groundwater scheme, further details can be found in previous studies (Fan et al., 2007 and Miguez-
 185 Macho et al., 2007).

186

187 [13] Fig. 2 is a diagram of the structure of Noah-MP soil layers and the MMF aquifer. The active
 188 2-m soil in Noah-MP LSM consists of 4 layers whose thicknesses (dz) are 0.1, 0.3, 0.6 and 1.0 m.
 189 The MMF scheme defines explicitly an unconfined aquifer below the 2-m soil and an auxiliary
 190 soil layer stretching to the WTD, which varies in space and time [m]. The thickness of this auxiliary
 191 layer (z_{aux} [m]) is also variable, depending on the WTD:

$$192 \quad z_{aux} = \begin{cases} 1, & WTD \geq -3 \\ -2 - WTD, & WTD < -3 \end{cases} \quad (1)$$

193

194 [14] Fig. 2 shows the soil layers of NoahMP coupled MMP groundwater scheme. The vertical
 195 fluxes include gravity drainage and capillary flux, solved from the Richards' equation,

$$196 \quad q = K_{SMC} * \left(\frac{\partial \Psi}{\partial z} - 1 \right), \quad K_{SMC} = K_{SAT} * \left(\frac{SMC}{SMCSAT} \right)^{2b+3}, \quad \Psi = \Psi_{SAT} * \left(\frac{SMCSAT}{SMC} \right)^b \quad (2)$$

197 where q is water flux between two adjacent layers [m/s], K_{SMC} is the hydraulic conductivity [m/s]
 198 at certain soil moisture content SMC [m³/m³], Ψ is the soil capillary potential [m] and b is soil pore
 199 size index. The subscript SAT denote saturated state whose values are from the default Noah-MP



200 soil tables. Therefore, the recharge flux from/to the layer above WTD, R , can be obtained
 201 according to WTD:

$$202 \quad R = \begin{cases} K_k * \left(\frac{\Psi_i - \Psi_k}{z_{soil(i)} - z_{soil(k)}} - 1 \right), & WTD \geq -2 \\ K_{aux} * \left(\frac{\Psi_4 - \Psi_{aux}}{(-2) - (-3)} - 1 \right), & -2 > WTD \geq -3 \\ K_{SAT} * \left(\frac{\Psi_{aux} - \Psi_{SAT}}{(-2) - (WTD)} - 1 \right), & WTD < -3 \end{cases} \quad (3)$$

203 In the first case, WTD is in the resolved soil layers and z_{soil} is the depth of soil layer with the
 204 subscript k indicating the layer containing WTD while i the layer above. The calculated water table
 205 recharge is then passed to the MMF groundwater routine.

206

207 [15] The change of groundwater storage in the unconfined aquifer considers three components:
 208 recharge flux, river flux, and lateral flows:

$$209 \quad \Delta S_g = (R - Q_r + \sum Q_{lat}) \quad (4)$$

210 where S_g [mm] is groundwater storage, Q_r [mm] is the water flux of groundwater-river exchange,
 211 and $\sum Q_{lat}$ [mm] are groundwater lateral flows to/from all surrounding grid cells (Fan et al., 2007;
 212 Miguez-Macho et al., 2007). The groundwater lateral flow ($\sum Q_{lat}$) is the total horizontal flows
 213 between each grid cell and its neighbouring grid cells, calculated from Darcy's law with the
 214 Dupuit–Forchheimer approximation (Fan and Miguez-Macho 2010), as:

$$215 \quad Q_{lat} = wT \left(\frac{h - h_n}{l} \right) \quad (5)$$

216 where w is the width of cell interface [m], T is the transmissivity of groundwater flow [m²/s], h
 217 and h_n are the water table head [m] of local and neighboring cell, and l is the length [m] between
 218 cells. T depends on hydraulic conductivity K and WTD:



$$T = \begin{cases} \int_{-\infty}^h K dz & WTD \geq -2 \\ \int_{-\infty}^{(z_{surf}-2)} K dz + \sum K_i * dz_i & WTD < -2 \end{cases} \quad (7)$$

219 For $WTD < -2$, K is assumed to decay exponentially with depth, $K = K_4 \exp(-z/f)$, K_4 is the
 220 hydraulic conductivity in the 4-th soil layer and f is the e-folding length and depends on terrain
 221 slope. For $WTD \geq -2$, i represents the number of layers between the water table and the 2-m bottom
 222 and z_{surf} is the surface elevation.
 223

224

225 [16] The river flux (Q_r) is also represented by a Darcy's law-type equation, which is the gradient
 226 between the groundwater head, local riverbed depth and parameterized river conductance:

$$Q_r = RC \cdot (h - z_{river}) \quad (8)$$

228 with z_{river} is the depth of river bed [m] and RC is dimensionless river conductance, which depends
 229 on the slope of the terrain and equilibrium water table ($eqzwt$, [m]). Eq. (7) is a simplification
 230 which uses z_{river} rather than the water level in the river and, for this study, we only consider one-
 231 way discharge from groundwater to rivers. Finally, the change of WTD is calculated as the total
 232 fluxes fill or drain the pore space between saturation and the equilibrium soil moisture state
 233 ($SMCEQ$ [m^3/m^3]) in the layer containing WTD:

$$\Delta WTD = \frac{\Delta S_g}{(SMCSAT - SMCEQ)} \quad (9)$$

235 If ΔS_g is greater than the pore space in the current layer, the soil moisture content of current layer
 236 is saturated and the WTD rises to the layer above, updating the soil moisture content in the layer
 237 above as well. Vice versa for negative ΔS_g as water table declines and soil moisture decreases.

238



239 **Fig. 2** Structure of the Noah-MP LSM coupled with MMF groundwater scheme, the top 2-m soil is consist of 4 layers
240 whose depth are 0.1, 0.3, 0.6 and 1.0 m. An unconfined aquifer is added below the 2-m boundary, including an
241 auxiliary layer and the saturated aquifer. Positive flux of R denotes downward transport. Two water table are shown,
242 one within the 2-m soil and one below, indicating that the model is capable to deal with shallow as well as deep water
243 table.
244



245 2.3 Forcing Data

246 [17] We use the atmospheric forcing from the WRF CONUS simulation (Liu et al. 2017) to drive
247 the Noah-MP-MMF model. The WRF CONUS simulation consists of two parts: one is the current
248 climate scenario from Oct 2000 to Sep 2013, downscaled from ERA-Interim reanalysis data; the
249 other is the pseudo global warming (PGW) as the future climate scenario, which adds a delta
250 climate change signal derived from an ensemble of CMIP5 models.

251

252 [18] **Fig. 3** shows the annual precipitation in the PPR from 4-km WRF CONUS from the current
253 climate and 32-km North America Regional Reanalysis (NARR, another reanalysis dataset
254 commonly used for land surface model forcing). Both datasets show similar annual precipitation
255 pattern and bias patterns compared to observations: underestimating of precipitation in the east
256 and overestimating in the west. However, the WRF CONUS shows significant improvement of
257 percentage bias in precipitation $((\text{Model-Observation})/\text{Observation})$ over the western PPR. To also
258 address the consistency of using the same source of data for current and future climate, we believe
259 the 4-km WRF CONUS is the best available dataset to drive the coupled land-groundwater model.

260

261 **Fig. 3** Evaluation of the annual precipitation from WRF CONUS (top) and NARR (bottom) against rain gauge
262 observation.

263

264 [19] For the future climate study, the precipitation and temperature of the PGW climate forcing
265 are shown in **Fig. 4** and **Fig. 5**. The WRF CONUS projects more precipitation in the PPR, except
266 in the southeast of the domain in summer, where it shows a precipitation reduction of about 50 to
267 100 mm. On the other hand, the WRF CONUS projects strongest warming occurring in the
268 northeast PPR in winter (**Fig. 5**) – warming of about 6–8 °C. Another significant warming signal



269 occurs in summer in the southeast of domain, corresponding to the reduction of future precipitation,

270 as seen in **Fig. 4**.

271

272 **Fig. 4** Seasonal accumulated precipitation from current climate scenario(CTRL), future climate scenario (PGW) and

273 projected change (PGW-CTRL) in the forcing data.

274

275 **Fig. 5** Same as **Fig. 4** but for 2-m air temperature.

276



277 2.4 Model Setup

278 [20] The two Noah-MP-MMF simulations representing the current climate and future climate are
279 denoted as CTRL and PGW, respectively. The CTRL simulation starts from Oct 2000 and end in
280 Sep 2013, consist of 13 water years. The PGW simulation corresponds to the same period of time,
281 but under climate change scenario at the end of 21st century.

282

283 [21] The model's initial groundwater is from a global 1-km equilibrium groundwater map (Fan et
284 al., 2013) and the equilibrium soil moisture for each soil layer is calculated at the first model
285 timestep with climatology recharge, spinning up for 500 years. Since the model domain is at a
286 different resolution than the input data, the appropriate initial WTD at 4-km may be different than
287 the average at 1-km. To properly initialize the simulation, we spin up the model using the forcing
288 of current climate (CTRL) for the years from 2000 to 2001 repeatedly (in total 4 loops).

289

290 [22] Due to different data sources, the default soil types along the boundary between the U.S. and
291 Canada are discontinuous. Thus, we use the global 1-km fine soil data (Shangguan et al., 2014,
292 <http://globalchange.bnu.edu.cn/research/soilw>) in our study region. The coupled Noah-MP-MMF
293 groundwater model is configured using the default 2-m depth with 4 layers. The soil properties for
294 the aquifer use the same properties as the lowest soil layer.



295 3. Results

296 3.1 Comparison with groundwater observations

297 [23] According to the locations of 11 groundwater wells in **Table 1**, the simulated WTD from the
298 closest model grid points are extracted. **Fig. 6** shows the observed WTD (black plus) and simulated
299 monthly WTD (blue lines) in the study domain. The model successfully captures the annual cycle
300 of WTD, which rises in spring and early summer, because of snowmelt and rainfall recharge, and
301 declines in summer and fall, because of high ET, and in winter because of frozen near-surface soil.
302 In all observations, the timing of water table rising and dropping is well simulated, as the timing
303 and amount of infiltration and recharge in spring is controlled by the freeze-thaw processes in
304 seasonally frozen soil. These processes are reasonably captured by the frozen soil scheme in Noah-
305 MP LSM (Niu et al., 2006; Niu et al., 2011).

306

307 **Fig. 6** WTD (m) from 11 groundwater wells and the model simulation results in the PPR.

308

309 [24] On the other hand, the model simulated WTD seasonal variation is smaller than observations.
310 The small seasonal variation could be due to the mismatch between the lithology from the
311 observational surveys and the soil types in the model grids. As mentioned in Section 2.2, the soil
312 properties of the unconfined aquifer are the same as the bottom layer of the resolved 2-m soil
313 layers. While sand and gravel are the dominant lithology in most of the sites, except for silt in
314 Crater Lake, they are mostly clay and loam in the model (Table 1). For sandy soil reported in most
315 of the sites, fast responses to infiltration and drainage lead to large water table fluctuations,
316 whereas, in the model, clay and loam soil allows low permeability and smoothens responses to
317 recharge and capillary effects. This shortcoming of the model was also reported in a study taken
318 place in the Amazon rainforest (Miguez-Macho et al., 2012).



319

320 [25] Despite mismatches between the model and sites in topography and soil properties at high
321 spatial resolution, this out-of-the-box simulation of the Noah-MP MMF groundwater scheme
322 shows reasonable results, as shown in **Fig. 6**. Therefore, we consider the simulated WTD
323 satisfactory in the mean, seasonal, and interannual dynamics, and are reliable for further study of
324 climate change impacts on groundwater in the PPR.

325



326 3.2 Climate change signal in Groundwater fluxes

327 [26] The MMF groundwater model simulates three components in the groundwater water budget,
328 the recharge flux (R), lateral flow (Q_{lat}), and discharge flux to rivers (Q_r). Because the topography
329 is usually flat in the PPR, the magnitude of groundwater lateral transport is very small (Q_{lat} less
330 than 5 mm per year). On the other hand, the shallow water table in the PPR region is higher than
331 the local river bed, thus, the Q_r term is always negative and discharging from groundwater aquifers
332 to rivers. As a result, the recharge term is the major contributor to the groundwater storage in the
333 PPR, and its variation (usually between -100 to 100 mm) dominates the timing and amplitude of
334 the water table dynamics. The seasonal accumulated total groundwater fluxes in the PPR
335 ($R+Q_{lat}+Q_r$) are shown in **Fig. 7**. The positive flux (blue) means the groundwater aquifer is
336 gaining water, causing the water table to rises; and the negative flux (red) indicates the aquifer is
337 losing water and the water table is declining.

338

339 **Fig. 7** Same as **Fig. 3** but for total groundwater fluxes ($R + Q_{lat} - Q_r$).

340

341 [27] Under current climate, the total groundwater flux show strong seasonal fluctuations,
342 consistent with the WTD timeseries shown in **Fig. 6**. On average, in fall (SON) and winter (DJF),
343 there is a 20-mm negative recharge, driven by the capillary effects and drawing water from aquifer
344 to dry soil above. Spring (MAM) is usually the season with a strong positive recharge because
345 snowmelt provides a significant amount of water, and soils thawing allow infiltration. The large
346 amount of snowmelt water contributes to more than 100 mm of positive recharge in the eastern
347 domain. It is until summer (JJA), when strong ET depletes soil moisture and results in about 50
348 mm of negative recharge.

349



350 [28] Under future climate, the increased PR in fall and winter leads to wetter upper soil layers,
351 resulting in a net positive recharge flux (PGW – CTRL in SON and DJF). However, the PGW
352 summer is impacted by increased ET under a warmer and drier climate, due to higher temperature
353 and less PR. As a result, the groundwater uptake by the capillary effect is more critical in the future
354 summer. Furthermore, there is a strong east-to-west difference in the total groundwater flux change
355 from PGW to CTRL. In the eastern PPR, the change in total groundwater flux exhibits obvious
356 seasonality while the model projects persistent positive groundwater fluxes in the western PPR.
357



358 3.3 Water budget analysis

359 [29] **Fig. 8** and **Fig. 9** show the water budget analysis for the eastern and western PPR (divided by
360 the dotted line in 103° W in Fig. 7), respectively. Four components are presented in the figures,
361 i.e. (1) PR and ET; (2) surface and underground runoff (*SFCRUN* and *UDGRUN*); and surface
362 snowpack; (3) the change of soil moisture storage and (4) groundwater fluxes and the change of
363 storage. In current and future climate, these budget terms are plotted in annual accumulation ((a)
364 and (b) for CTRL and PGW), whereas their difference are plotted in each month individually ((c)
365 for PGW-CTRL).

366

367 [30] During snowmelt infiltration and rainfall events when ET demand is low, water infiltrates into
368 the top soil layer, travels through the soil column and exits the bottom of the 2-m boundary, hence,
369 the water table rises. During the summer dry season, ET is higher than PR and the soil layers lose
370 water through ET, therefore, the capillary effect takes water from the underlying aquifer and the
371 water table declines. In winter, the near-surface soil in the PPR is seasonally frozen, thus, a
372 redistribution of subsurface water to the freezing front results in negative Q_{drain} , and the water
373 table declines.

374

375 [31] In the eastern PPR, the effective precipitation (PR-ET) is found to increase from fall to spring,
376 but decrease in summer in PGW (**Fig. 8(1c)**). Warmer falls and winters in PGW, together with
377 increased PR, not only results in later time for snow accumulation and earlier for melting, but also
378 changes the precipitation partition – more as rain and less as snow. This warming causes up to 20
379 mm of snowpack loss (**Fig.8(2c)**). The underground runoff starts much earlier in PGW (December)
380 (**Fig.8(2b)**) than in CTRL (February) (**Fig.8(2a)**). On the other hand, the warming in PGW also



381 changes the partitioning of soil ice and soil water in subsurface soil layers (**Fig. 8(3c)**). For late
382 spring in PGW, the springtime recharge in the future is significantly reduced due to early melting
383 and less snowpack remaining (**Fig. 8(4c)**). In the PGW summer, reduced PR (50 mm less) and
384 higher temperatures (8 °C warmer) lead to reduction in total soil moisture, and a stronger negative
385 recharge from the aquifer. Therefore, the increase of recharge from fall to early spring compensates
386 the recharge reduction due to stronger ET in summer in the eastern PPR, and changes little in the
387 annual mean groundwater storage (1.763 mm per year).

388

389 **Fig. 8** Water budget analysis in the eastern PPR in (a) CTRL, (b) PGW and (c) PGW – CTRL. Water budget terms
390 include: (1) *PR & ET*, (2) surface snow, surface runoff and underground runoff (*SNOW*, *SFCRUN*, and *UDGRUN*),
391 (3) change of soil moisture storage (soil water, soil ice and total soil moisture, ΔSMC) and (4) groundwater fluxes
392 and the change of groundwater storage (R , Q_{lat} , Q_r , ΔS_g). The annual mean soil moisture change (PGW-CTRL) is
393 shown with black dashed line in (3). The Residual term is defined as $Res = (R+Q_{lat}-Q_r)-\Delta S_g$ in (4). Note that in (a)
394 and (b) the accumulated fluxes and change in storage are shown in lines, whereas in (c) the difference in (PGW-CTRL)
395 is shown for each individual month in bars.

396

397 [32] These changes in water budget components in the western PPR (**Fig. 9**) are similar to those
398 in the eastern PPR (**Fig. 8**), except in summer. The reduction in summer PR in the western the PPR
399 (less than 5 mm reduction) is not as obvious as that in the eastern PPR (50 mm reduction) (**Fig. 4**).
400 Thus, annual mean total soil moisture in future is about the same as in current climate (Fig. 9(3c))
401 and results in little negative recharge in PGW summer (**Fig. 9(4c)**). Therefore, the increase in
402 annual recharge is more significant (10 mm per year), an increase of about 50% of the annual
403 recharge in the current climate (20 mm per year) (**Fig. 9(4c)**).

404

405 **Fig. 9** Same as **Fig. 8**, but for the western PPR.



406

407 [33] In both the eastern and western PPR, the water budget components for the groundwater aquifer
408 are plotted in **Fig. 8(4)** and **Fig. 9 (4)**, with the changes of each flux (PGW-CTRL) printed at the
409 bottom. The groundwater lateral flow is a small term in areal average and has little impact on the
410 groundwater storage. Nearly half of the increased recharge in both the eastern and western PPR is
411 discharged to river flux ($Q_r = 2.26$ mm out of $R = 4.15$ mm in the eastern PPR and $Q_r = 5.20$ mm
412 out of $R = 10.72$ mm in western PPR). Therefore, the groundwater storage change in the eastern
413 PPR (1.76 mm per year) is not as great as that in the western PPR (5.39 mm per year).

414

415 [34] These two regions of the PPR show differences in hydrological response to future climate
416 because of the spatial variation of the summer PR. As shown in both **Fig. 4** (PGW-CTRL), **Fig.**
417 **8(1)** and **Fig. 9(1)**, the reduction of future PR in summer in the eastern PPR is significant (50 mm).
418 The spatial difference of precipitation changes in the PPR further results in the recharge increase
419 doubling in the western PPR compared to the eastern PPR.

420



421 4. Discussion

422 4.1 Simulated WTD sensitivity to soil property parameters

423 [35] In Section 3.1, we show that model is capable of simulating the mean WTD, yet
424 underestimates its seasonal variation due to mismatches between model default soil type and the
425 soil properties in the observational wells. To test this theory, an additional simulation, REP, is
426 conducted by replacing the default soil types in the 11 sites with the dominant soil types reported
427 from observational surveys. The time series of the REP and default (MOD) are shown in Fig. 10
428 and a summary of the mean and standard deviation of the two simulations are provided in Table 2.

429

430 **Fig. 10** Same as Fig. 6, the time series of simulated WTD from both default model (MOD) and replacing soil type
431 simulation (REP).

432

433 [36] The REP simulation with soil type from observational surveys show two sensitive signals: (1)
434 REP WTD (red lines in Fig. 10) are shallower than the default simulation; (2) REP WTD timeseries
435 shows stronger seasonal variation. These two signals can be explained by the WTD equation in
436 the MMF scheme:

$$437 \quad \Delta WTD = \frac{\Delta(R + Q_{lat} + Q_r)}{(SMCSAT - SMCEQ)} \quad (10)$$

438 where $SMCMAX$ is the maximum soil moisture capacity in the current layer, a parameter
439 determined by the soil type. Eq. (10) represents that the change of WTD in a period of time is
440 calculated by the total groundwater fluxes, $\Delta(R + Q_{lat} + Q_r)$, divided by the available soil
441 moisture capacity of current layer ($SMCMAX - SMCEQ$). In REP simulation, the $SMCSAT$
442 parameters for the dominant soil type in observational sites (sand/gravel) is smaller than those in
443 default model grids (clay loam, sandy loam, loam, loamy sand, etc.). Therefore, changing the



444 *SMCSAT* is essentially altering the storage in the aquifer and soil in this model grid. Given the
445 same amount of groundwater flux, in the REP simulation, the mean WTD is higher than the default
446 run and the seasonal variation is stronger, hence, increasing the WTD seasonal variation.

447

448 [37] We show the REP simulation in order to prove our theory in Section 3.1, that the simulated
449 WTD is sensitive to parameters associated soil properties, and thus could be improved by obtaining
450 more realistic soil maps. But in the REP simulation, we replaced soil type with observations only
451 at these 11 site locations because the geological survey data in high resolution and large area extent
452 is not yet available for the whole PPR. Future development in fine-scale soil properties will
453 hopefully improve the WTD simulation.

454

455 4.2 Climate change Impacts on Groundwater Hydrologic Regime

456 [38] Climate change induced warming in high-latitudes winter and increased precipitation,
457 including a higher liquid fraction, in PGW winter results in later snow accumulation, higher winter
458 recharge and earlier melting in spring. Such changes in snowpack loss have been hypothesized in
459 mountainous as well as high-latitude regions (Taylor et al 2013; Ireson et al., 2015; Meixner et al.,
460 2016; Musselman et al., 2017). On an annual basis, the coupled model projects substantial
461 increases in recharge, 25% in eastern and 50% in western PPR.

462

463 [39] In addition to the amount of recharge, the shift of recharge season is also noteworthy. Under
464 current climate in spring, soil thawing (in March) is generally later than snowmelt (in February)
465 by a month in the PPR. Thus, the snowmelt water in pre-thaw spring would either re-freeze after
466 infiltrating into partially frozen soil or become surface runoff. Under the PGW climate, the warmer



467 winter and spring allows snowmelt and soil thaw to occur earlier in the middle of winter (in January
468 and February, respectively). As a result, the recharge season starts earlier in December, and last
469 longer until June, results in longer recharge season but with lower recharge rate.

470

471 [40] Future projected stronger evapotranspiration demand in summer desiccates upper soil layers,
472 resulting in more water uptake from aquifers to subsidize upper dry soil in the future summer. This
473 groundwater transport to upper soil layers is similar to the “buffer effect” documented in an offline
474 study in the Amazon rainforest. In both Amazon rainforest and the PPR, shallow water tables exist
475 in the critical zone from 1 to 5 meters below surface (Kollet and Maxwell, 2008; Fan , 2015) and
476 could exert strong influence on land energy and moisture fluxes feedback to the atmosphere.
477 Previous coupled atmosphere-land-groundwater studies at 30-km resolution showed that
478 groundwater could support soil moisture during summer dry period, but has little impacts on
479 precipitation in Central U.S. (Barlage et al., 2015). It would be an interesting topic to study the
480 integrated impacts of shallow groundwater to regional climate in the convection permitting
481 resolution (resolution < 5-km).

482



483 Conclusion

484 [41] The fluctuation of the shallow WTD and recharge are closely related to the semi-arid climatic
485 condition and seasonally frozen soil in the Prairie Pothole Region (PPR). The freeze-thaw
486 processes and effective precipitation are critical factors to the magnitude and timing for snowmelt
487 infiltration in spring, groundwater uptake in summer and moisture redistribution in winter. The
488 two-way water exchange between soil layers and groundwater aquifer is essential to the
489 groundwater regime in the PPR.

490

491 [42] Previous works on modeling climate change impacts on groundwater, at both global or local
492 basin scale, have been limited by precipitation uncertainties stemming from choice of convection
493 parameterization in GCMs. (Green et al., 2011; Kurylyk et al., 2013; Taylor et al., 2013; Smerdon
494 2017). Additionally, these models typically neglected the two-way exchange of water flux between
495 soil and aquifers, which has been a historical simplification in the coupled land-groundwater model.

496

497 [43] In our study, a coupled land-groundwater model is applied to simulate the interaction between
498 the groundwater aquifer and soil moisture in the PPR. The climate forcing is from a dynamical
499 downscaling project (WRF CONUS), which uses the high spatial resolution convection-permitting
500 model (CPM). To our knowledge, this is the first study applying convection-permitting regional
501 climate model (RCM) forcing in a hydrology study. The goal of this study is to investigate the
502 groundwater responses to climate change, and to identify the major processes that contribute to
503 these responses in the PPR. We have three main findings:

504



505 [44] (1) the coupled land-groundwater model shows reliable simulation of mean WTD, however
506 underestimates the seasonal variation of the water table against well observations. This is mostly
507 due to the mismatches of soil types between groundwater sites and corresponding model grid
508 points. This mismatch comes from inadequate information of aquifer parameters, which are the
509 same as those for the lowest soil layer. We further demonstrated in an additional simulation (REP)
510 by replacing the default soil type with observational “true” value that the simulated WTD is
511 sensitive to soil type parameters, and the simulated WTDs were improved in both mean and
512 seasonal variation. However, inadequacy of soil properties in deeper layer (< -2 m) is still a
513 limitation.

514

515 [45] (2) In general, recharge markedly increases due to projected increased PR, particularly from
516 fall to spring under future climate condition. Strong east-west spatial variation exists in the annual
517 recharge increases, 25% in the eastern and 50% in the western PPR. This is due to the significant
518 projected PR reduction in PGW summer in the eastern PPR but little change in the western PPR.
519 This PR reduction results in stronger ET, which draws more groundwater uptake due to the
520 capillary effect, results in negative recharge in the summer. As a results, the increased recharge
521 from fall to spring is consumed by ET in summer, and results in little change in groundwater
522 storage in the eastern PPR, while higher storage in the western PPR.

523

524 [46] (3) The timing of infiltration and recharge are critically impacted by the changes in
525 temperature-induced freeze-thaw processes. Increased precipitation, combined with higher winter
526 temperatures, results in later snow accumulation/soil freezing, partitioned more as rain than snow,
527 and earlier snowmelt/soil thaw. This leads to substantial loss of snowpack, shorter frozen soil



528 season, and higher permeability in soil allowing infiltration in the future winter. Additionally, late
529 accumulation/freezing and early melting/thawing leads to an early start of a longer recharge season
530 from December to June, but with a lower recharge rate.

531

532 [47] Our study has some limitations where future studies are needed:

533 (1) Despite the large number of groundwater wells in PPR, only a few are suitable for long-term
534 evaluation, due to data quality, anthropogenic pumping, and length of data record. As remote
535 sensing techniques advance, observing terrestrial water storage anomalies derived from the
536 GRACE satellite may provide substantial information on WTD, although the GRACE information
537 needs to be downscaled to a finer scale before comparisons can be made with regional hydrology
538 models at km-scale (Pokhrel et al., 2013).

539

540 [48] (2) This study is an offline study of climate change impacts on groundwater. It is important
541 to investigate how shallow groundwater in the earth's critical zone could interact with surface
542 water and energy exchange to the atmosphere and affect regional climate. This investigation would
543 be important to the central North America region (one of the land atmosphere coupling "hot spots",
544 Koster et al., 2004).

545



546 **Acknowledgments**

547 The authors Zhe Zhang, Yanping Li, Zhenhua Li gratefully acknowledge the support from the
548 Changing Cold Regions Network (CCRN) funded by the Natural Science and Engineering
549 Research Council of Canada (NSERC), as well as the Global Water Future project and Global
550 Institute of Water Security at University of Saskatchewan. Yanping Li acknowledge the support
551 from NSERC Discovery Grant. Fei Chen, Michael Barlage appreciate the support from the Water
552 System Program at the National Center for Atmospheric Research (NCAR), USDA NIFA Grants
553 2015-67003-23508 and 2015-67003-23460, NSF INFEW/T2 Grant #1739705, and NOAA CFDA
554 Grant #NA18OAR4590381. NCAR is sponsored by the National Science Foundation. Any
555 opinions, findings, conclusions or recommendations expressed in this publication are those of the
556 authors and do not necessarily reflect the views of the National Science Foundation.

557



558 Reference

- 559 Anyah, R. O., Weaver, C. P., Miguez-macho, G., Fan, Y. and Robock, A.: Incorporating water
560 table dynamics in climate modeling : 3 . Simulated groundwater influence on coupled land-
561 atmosphere variability, , 113, 1–15, doi:10.1029/2007JD009087, 2008.
- 562 Ban, N., Schmidli, J. and Schär, C.: Evaluation of the new convective-resolving regional climate
563 modeling approach in decade-long simulations, *J. Geophys. Res. Atmos.*, 119, 7889–7907,
564 doi:10.1002/2014JD021478.Received, 2014.
- 565 Barlage, M., Tewari, M., Chen, F., Miguez-Macho, G., Yang, Z. L. and Niu, G. Y.: The effect of
566 groundwater interaction in North American regional climate simulations with WRF/Noah-MP,
567 *Clim. Change*, 129(3–4), 485–498, doi:10.1007/s10584-014-1308-8, 2015.
- 568 Brannen, R., Spence, C. and Ireson, A.: Influence of shallow groundwater-surface water
569 interactions on the hydrological connectivity and water budget of a wetland complex, *Hydrol.*
570 *Process.*, 29(18), 3862–3877, doi:10.1002/hyp.10563, 2015.
- 571 Döll, P. and Fiedler, K.: Global-scale modeling of groundwater recharge, *Hydrol. Earth Syst. Sci.*,
572 12(3), 863–885, doi:10.5194/hess-12-863-2008, 2008.
- 573 Döll, P.: Vulnerability to the impact of climate change on renewable groundwater resources: A
574 global-scale assessment, *Environ. Res. Lett.*, 4(3), doi:10.1088/1748-9326/4/3/035006, 2009.
- 575 Dumanski, S., Pomeroy, J. W. and Westbrook, C. J.: Hydrological regime changes in a Canadian
576 Prairie basin, *Hydrol. Process.*, 29(18), 3893–3904, doi:10.1002/hyp.10567, 2015.
- 577 Environment Canada: Municipal Water Use, 2009 Statistics, 2011 Munic. Water Use Rep., 24,
578 doi:En11-2/2009E-PDF Information, 2011.
- 579 Fan Y, Miguez-Macho G, Weaver CP, et al (2007) Incorporating water table dynamics in climate
580 modeling: 1. Water table observations and equilibrium water table simulations. *J Geophys*
581 *Res Atmos* 112:1–17. doi: 10.1029/2006JD008111
- 582 Fan, Y., Li, H. and Miguez-Macho, G.: Global patterns of groundwater table depth, *Science* (80-.),
583 339(6122), 940–943, doi:10.1126/science.1229881, 2013.
- 584 Fan, Y.: Groundwater in the Earth’s critical zones: Relevance to large-scale patterns and processes,
585 *Water Resour. Res.*, 3052–3069, doi:10.1002/2015WR017037.Received, 2015.
- 586 Granger RJ, Gray DM: Evaporation from natural non-saturated surface. *J. Hydrol.*, 111, 21–29,
587 1989.
- 588 Gray DM: Handbook on the Principles of Hydrology: With Special Emphasis Directed to Canadian
589 Conditions in the Discussion, Applications, and Presentation of Data. Water Information
590 Center: Huntington, New York, 1970. ISBN:0-912394-07-2
- 591 Green, T. R., Taniguchi, M., Kooi, H., Gurdak, J. J., Allen, D. M., Hiscock, K. M., Treidel, H. and
592 Aureli, A.: Beneath the surface of global change: Impacts of climate change on groundwater,
593 *J. Hydrol.*, 405(3–4), 532–560, doi:10.1016/j.jhydrol.2011.05.002, 2011.
- 594 Hayashi, M., Van Der Kamp, G. and Schmidt, R.: Focused infiltration of snowmelt water in
595 partially frozen soil under small depressions, *J. Hydrol.*, 270(3–4), 214–229,
596 doi:10.1016/S0022-1694(02)00287-1, 2003.
- 597 Hayashi, M., van der Kamp, G. and Rosenberry, D. O.: Hydrology of Prairie Wetlands:
598 Understanding the Integrated Surface-Water and Groundwater Processes, *Wetlands*, 36, 237–
599 254, doi:10.1007/s13157-016-0797-9, 2016.
- 600 Ireson, A. M., van der Kamp, G., Ferguson, G., Nachshon, U. and Wheater, H. S.: Hydrogeological
601 processes in seasonally frozen northern latitudes: understanding, gaps and challenges,
602 *Hydrogeol. J.*, 21(1), 53–66, doi:10.1007/s10040-012-0916-5, 2013.



- 603 Ireson, A. M., Barr, A. G., Johnstone, J. F., Mamet, S. D., van der Kamp, G., Whitfield, C. J.,
604 Michel, N. L., North, R. L., Westbrook, C. J., DeBeer, C., Chun, K. P., Nazemi, A. and Sagin,
605 J.: The changing water cycle: the Boreal Plains ecozone of Western Canada, *Wiley Interdiscip.*
606 *Rev. Water*, 2(5), 505–521, doi:10.1002/wat2.1098, 2015.
- 607 Johnson, W. C., Werner, B., Guntenspergen, G. R., Voldseth, R. A., Millett, B., Naugle, D. E.,
608 Tulbure, M., Carroll, R. W. H., Tracy, J. and Olawsky, C.: Prairie Wetland Complexes as
609 Landscape Functional Units in a Changing Climate, *Bioscience*, 60(2), 128–140,
610 doi:10.1525/bio.2010.60.2.7, 2010.
- 611 Kelln C, Barbour L, Qualizza C (2007) Preferential Flow in a Reclamation Cover : Hydrological
612 and Geochemical Response. 1277–1289
- 613 Koster, R. D., Dirmeyer, P. A., Guo, Z., Bonan, G., Chan, E., Cox, P., Gordon, C. T., Kanae, S.,
614 Kowalczyk, E., Lawrence, D., Liu, P., Lu, C.-H., Malyshev, S., McAvaney, B., Mitchell,
615 K., Mocko, D., Oki, T., Oleson, K., Pitman, A., Sud, Y. C., Taylor, C. M., Verseghy, D.,
616 Vasic, R., Xue, Y. and Yamada, T.: Regions of Strong Coupling Between Soil Moisture and
617 Precipitation, *Science* (80-.), 305(5687), 1138 LP-1140 [online] Available from:
618 <http://science.sciencemag.org/content/305/5687/1138.abstract>, 2004.
- 619 Kollet SJ, Maxwell RM (2008) Capturing the influence of groundwater dynamics on land surface
620 processes using an integrated, distributed watershed model. *Water Resour Res* 44:1–18. doi:
621 10.1029/2007WR006004
- 622 Kurylyk, B. L. and MacQuarrie, K. T. B.: The uncertainty associated with estimating future
623 groundwater recharge: A summary of recent research and an example from a small unconfined
624 aquifer in a northern humid-continental climate, *J. Hydrol.*, 492, 244–253,
625 doi:10.1016/j.jhydrol.2013.03.043, 2013.
- 626 Liu, C., Ikeda, K., Rasmussen, R., Barlage, M., Newman, A. J., Prein, A. F., Chen, F., Chen, L.,
627 Clark, M., Dai, A., Dudhia, J., Eidhammer, T., Gochis, D., Gutmann, E., Kurkute, S., Li, Y.,
628 Thompson, G. and Yates, D.: Continental-scale convection-permitting modeling of the current
629 and future climate of North America, *Clim. Dyn.*, 49(1–2), 71–95, doi:10.1007/s00382-016-
630 3327-9, 2017.
- 631 Martinez, J. A., Dominguez, F. and Miguez-Macho, G.: Effects of a Groundwater Scheme on the
632 Simulation of Soil Moisture and Evapotranspiration over Southern South America, *J.*
633 *Hydrometeorol.*, 17(11), 2941–2957, doi:10.1175/JHM-D-16-0051.1, 2016.
- 634 Maxwell RM, Miller NL (2005) Development of a Coupled Land Surface and Groundwater
635 Model. 233–247
- 636 Maxwell, R. M. and Kollet, S. J.: Interdependence of groundwater dynamics and land-energy
637 feedbacks under climate change, *Nat. Geosci.*, 1(10), 665–669, doi:10.1038/ngeo315, 2008.
- 638 Meixner, T., Manning, A. H., Stonestrom, D. A., Allen, D. M., Ajami, H., Blasch, K. W.,
639 Brookfield, A. E., Castro, C. L., Clark, J. F., Gochis, D. J., Flint, A. L., Neff, K. L., Niraula,
640 R., Rodell, M., Scanlon, B. R., Singha, K. and Walvoord, M. A.: Implications of projected
641 climate change for groundwater recharge in the western United States, *J. Hydrol.*, 534, 124–
642 138, doi:10.1016/j.jhydrol.2015.12.027, 2016.
- 643 Miguez-Macho, G., Fan, Y., Weaver, C. P., Walko, R. and Robock, A.: Incorporating water table
644 dynamics in climate modeling: 2. Formulation, validation, and soil moisture simulation, *J.*
- 645 Miguez-Macho, G. and Fan, Y.: The role of groundwater in the Amazon water cycle: 1. Influence
646 on seasonal streamflow, flooding and wetlands, *J. Geophys. Res. Atmos.*, 117(15), 1–30,
647 doi:10.1029/2012JD017539, 2012.



- 648 Moeck, C., Brunner, P. and Hunkeler, D.: The influence of model structure on groundwater
649 recharge rates in climate-change impact studies, *Hydrogeol. J.*, 24(5), 1171–1184,
650 doi:10.1007/s10040-016-1367-1, 2016.
- 651 Musselman, K. N., Clark, M. P., Liu, C., Ikeda, K. and Rasmussen, R.: Slower snowmelt in a
652 warmer world, *Nat. Clim. Chang.*, 7(February), 214–220, doi:10.1038/NCLIMATE3225,
653 2017.
- 654 National Research Council: Groundwater fluxes across inter- faces. The National Academy Press,
655 85 pp, 2003
- 656 Niu G, Yang Z, Dickinson RE, Gulden LE (2007) Development of a simple groundwater model
657 for use in climate models and evaluation with Gravity Recovery and Climate Experiment
658 data. 112:1–14. doi: 10.1029/2006JD007522
- 659 Niu, G. Y., Yang, Z. L., Mitchell, K. E., Chen, F., Ek, M. B., Barlage, M., Kumar, A., Manning,
660 K., Niyogi, D., Rosero, E., Tewari, M. and Xia, Y.: The community Noah land surface model
661 with multiparameterization options (Noah-MP): 1. Model description and evaluation with
662 local-scale measurements, *J. Geophys. Res. Atmos.*, 116(12), 1–19,
663 doi:10.1029/2010JD015139, 2011.
- 664 Pokhrel, Y. N., Fan, Y., Miguez-Macho, G., Yeh, P. J. F. and Han, S. C.: The role of groundwater
665 in the Amazon water cycle: 3. Influence on terrestrial water storage computations and
666 comparison with GRACE, *J. Geophys. Res. Atmos.*, 118(8), 3233–3244,
667 doi:10.1002/jgrd.50335, 2013.
- 668 Pomeroy, J. W.: The cold regions hydrological model: a platform for basing process representation
669 and model structure on physical evidence, *Hydrol. Process.*, 21, 2650–2667, doi:10.1002/hyp,
670 2007.
- 671 Prein, A. F., Gobiet, A., Suklitsch, M., Truhetz, H., Awan, N. K., Keuler, K. and Georgievski, G.:
672 Added value of convection permitting seasonal simulations, , 2655–2677,
673 doi:10.1007/s00382-013-1744-6, 2013.
- 674 Prein, A. F., Langhans, W., Fosser, G., Ferrone, A., Ban, N., Goergen, K., Keller, M., Tölle, M.,
675 Gutjahr, O., Feser, F., Brisson, E., Kollet, S., Schmidli, J., Van Lipzig, N. P. M. and Leung,
676 R.: A review on regional convection-permitting climate modeling: Demonstrations, prospects,
677 and challenges, *Rev. Geophys.*, 53(2), 323–361, doi:10.1002/2014RG000475, 2015.
- 678 Rasmussen, K. L., Prein, A. F., Rasmussen, R. M., Ikeda, K. and Liu, C.: Changes in the convective
679 population and thermodynamic environments in convection-permitting regional climate
680 simulations over the United States, *Clim. Dyn.*, (0123456789), 1–26, doi:10.1007/s00382-
681 017-4000-7, 2017.
- 682 Remenda VH, van der Kamp G, Cherry JA (1996) Use of vertical profiles of • 180 to constrain
683 estimates of hydraulic conductivity in a thick, unfractured aquitard. 32:2979–2987
- 684 Shangguan W, Dai Y, Duan Q, et al (2014) *Journal of Advances in Modeling Earth Systems*. J
685 *Adv Model Earth Syst* 6:249–263. doi: 10.1002/2013MS000293. Received
- 686 Sherwood, S. C., Bony, S. and Dufresne, J.: Spread in model climate sensitivity traced to
687 atmospheric convective mixing, , doi:10.1038/nature12829, 2014.
- 688 Siebert, S., Burke, J., Faures, J. M., Frenken, K., Hoogeveen, J., Döll, P. and Portmann, F. T.:
689 Groundwater use for irrigation - A global inventory, *Hydrol. Earth Syst. Sci.*, 14(10), 1863–
690 1880, doi:10.5194/hess-14-1863-2010, 2010.
- 691 Smerdon, B. D.: A synopsis of climate change effects on groundwater recharge, *J. Hydrol.*, 555,
692 125–128, doi:10.1016/j.jhydrol.2017.09.047, 2017.



- 693 Statistics Canada: Quarterly Estimates of the Population of Canada, the Provinces and the
694 Territories, 11-3, Catalogue 91-001, Ottawa, 1996
- 695 Taylor, R. G.: Ground water and climate change, , 3(November 2012),
696 doi:10.1038/NCLIMATE1744, 2013.
- 697 Tremblay, L., Larocque, M., Anctil, F. and Rivard, C.: Teleconnections and interannual variability
698 in Canadian groundwater levels, J. Hydrol., 410(3–4), 178–188,
699 doi:10.1016/j.jhydrol.2011.09.013, 2011.
- 700 UNESCO: Groundwater Resources of the Wrold and Their Use, edited by I. Zektser and L. Everett,
701 Paris., 2004.
- 702 Van Der Kamp G, Hayashi M (2009) Groundwater-wetland ecosystem interaction in the
703 semiarid glaciated plains of North America. *Hydrogeol J* 17:203–214. doi: 10.1007/s10040-
704 008-0367-1
- 705 Yang, Z. L., Niu, G. Y., Mitchell, K. E., Chen, F., Ek, M. B., Barlage, M., Longuevergne, L.,
706 Manning, K., Niyogi, D., Tewari, M. and Xia, Y.: The community Noah land surface model
707 with multiparameterization options (Noah-MP): 2. Evaluation over global river basins, J.
708 Geophys. Res. Atmos., 116(12), 1–16, doi:10.1029/2010JD015140, 2011.
- 709



710
 711
 712
 713
 714

Table and Figure

Table 1. Summary of the locations and aquifer type and soil type of the 11 selected wells.

| WELL NAME | WELL ID | PROV | LAT | LON | ELEV | ELEV_MOD | AQUIFER TYPE | LITHOLOGY | SOIL_MOD |
|--------------------|---------|------|--------|----------|-------|----------|--------------|------------------|------------|
| Narrow Lake | 252 | AB | 54.600 | -113.631 | 640.0 | 701.0 | Surficial | Sand | Clay loam |
| Beauval | Beau | SK | 55.117 | -107.745 | 434.3 | 446.5 | Intertill | Sand | Sandy loam |
| Crater lake | Crat | SK | 50.953 | -102.463 | 524.1 | 522.8 | Intertill | Sand/Gravel/Silt | Loam |
| Duck lake | Duck | SK | 52.921 | -106.233 | 502.9 | 501.729 | Surficial | Sand | Loamy sand |
| Forget | Forg | SK | 49.705 | -102.863 | 606.5 | 606.0 | Surficial | Sand | Sandy loam |
| Simpson 14 | SI14 | SK | 51.457 | -105.193 | 496.6 | 493.3 | Surficial | Sand | Sandy loam |
| Yorkton No.517 | Y517 | SK | 51.173 | -102.509 | 513.6 | 511.2 | Surficial | Sand/Gravel | Loam |
| Prairie Island | PI98-14 | MN | 44.698 | 92.705 | 209.7 | 247.6 | Surficial | Sand/Gravel | Loamy sand |
| CRN Well | WLN03 | MN | 45.983 | 95.203 | 410.7 | 411.4 | Surficial | Sand/Gravel | Sandy loam |
| Glacial Ridge Well | G15 | MN | 47.635 | 96.254 | 351.7 | 344.2 | Surficial | Sand/Gravel | Loam sand |
| Glacial Ridge Well | E03 | MN | 47.738 | 96.235 | 341.9 | 336.2 | Surficial | Sand/Gravel | Sandy loam |

715



716 **Table 2.** Summary of mean and standard deviation (in the parenthesis) of WTD from 11
 717 groundwater wells, from observation records, default model (MOD) and replacing “true” soil
 718 properties simulation (REP). Bold texts show improvement in the mean and seasonal variation of
 719 WTD.

720

| STATION | BEAU | NARR 252 | DUCK | SI14 | FORG | Y517 | CRAT | GWR E03 | GRW G15 | CRN WLN03 | PI98- 14 |
|---------|-------------------------------|-------------------------------|------------------------|------------------------|-------------------------------|-----------------------|------------------------|-------------------------------|-------------------------------|-------------------------------|-------------------------------|
| OBS | -3.78 (0.44) | -2.31 (0.28) | -3.66 (0.54) | -2.03 (0.34) | -2.28 (0.33) | -2.87 (0.80) | -4.33 (1.10) | -2.44 (0.39) | -1.94 (0.39) | -2.04 (0.24) | -4.31 (0.53) |
| MOD | -4.85 (0.56) | -4.81 (0.60) | -4.21 (0.42) | -2.61 (0.18) | -2.70 (0.19) | -3.97 (0.46) | -3.97 (0.40) | -2.29 (0.21) | -2.32 (0.20) | -2.18 (0.18) | -4.52 (0.12) |
| REP | -4.20 (0.32) | -3.75 (0.51) | -3.54 (0.61) | -1.82 (0.27) | -1.66 (0.46) | 1.98 (0.32) | -3.64 (0.28) | -1.96 (0.40) | -2.26 (0.22) | -1.88 (0.43) | -4.43 (0.16) |

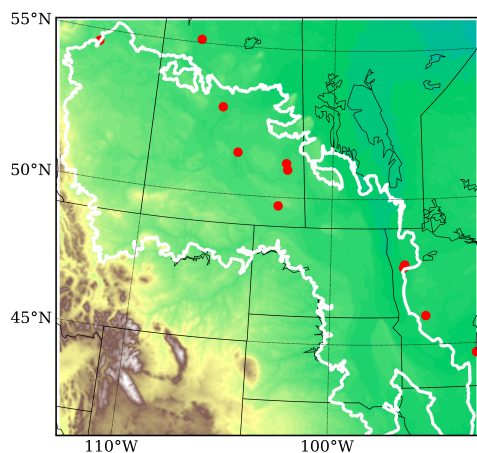
721

722

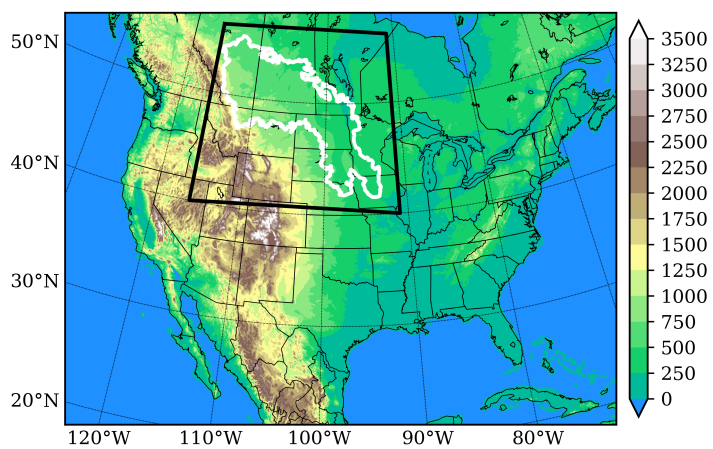


723

724 (a)



(b)



725

726

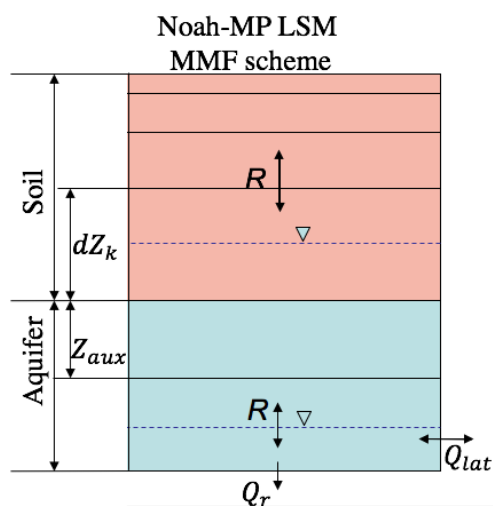
727

728

Fig. 1 (a) Topography of the Prairie Pothole Region (PPR; white outline) and station location of rain gauges (gray dots) and groundwater wells (red dots); (b) Topography of the WRF CONUS domain, the black box indicates the PPR domain.



729



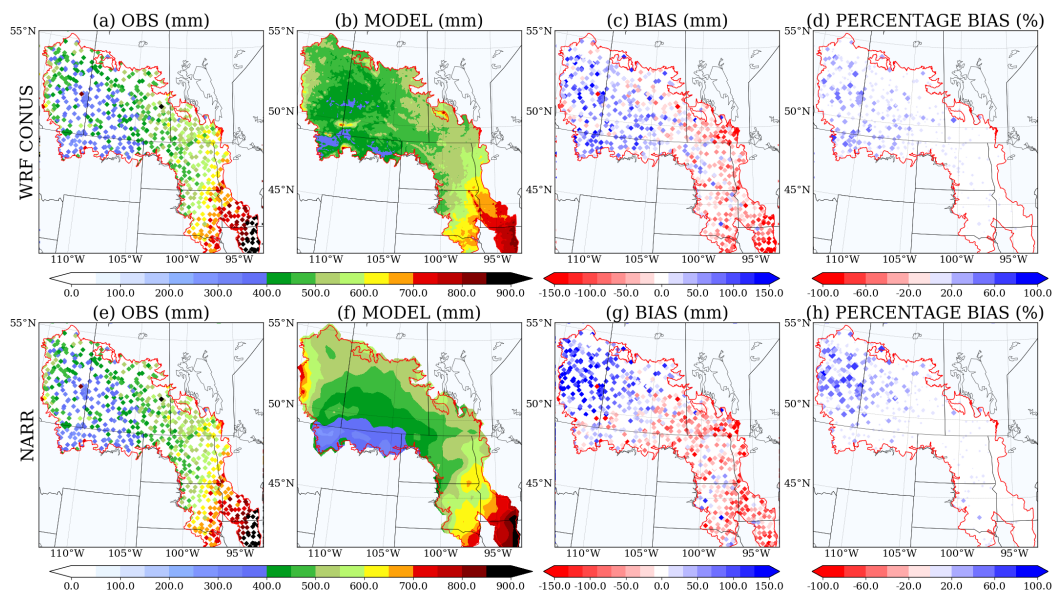
730

731 **Fig. 2** Structure of the Noah-MP LSM coupled with MMF groundwater scheme, the top 2-m soil is consist of 4 layers
732 whose depth are 0.1, 0.3, 0.6 and 1.0 m. An unconfined aquifer is added below the 2-m boundary, including an
733 auxiliary layer and the saturated aquifer. Positive flux of R denotes downward transport. Two water table are shown,
734 one within the 2-m soil and one below, indicating that the model is capable to deal with shallow as well as deep water
735 table.

736



737



738

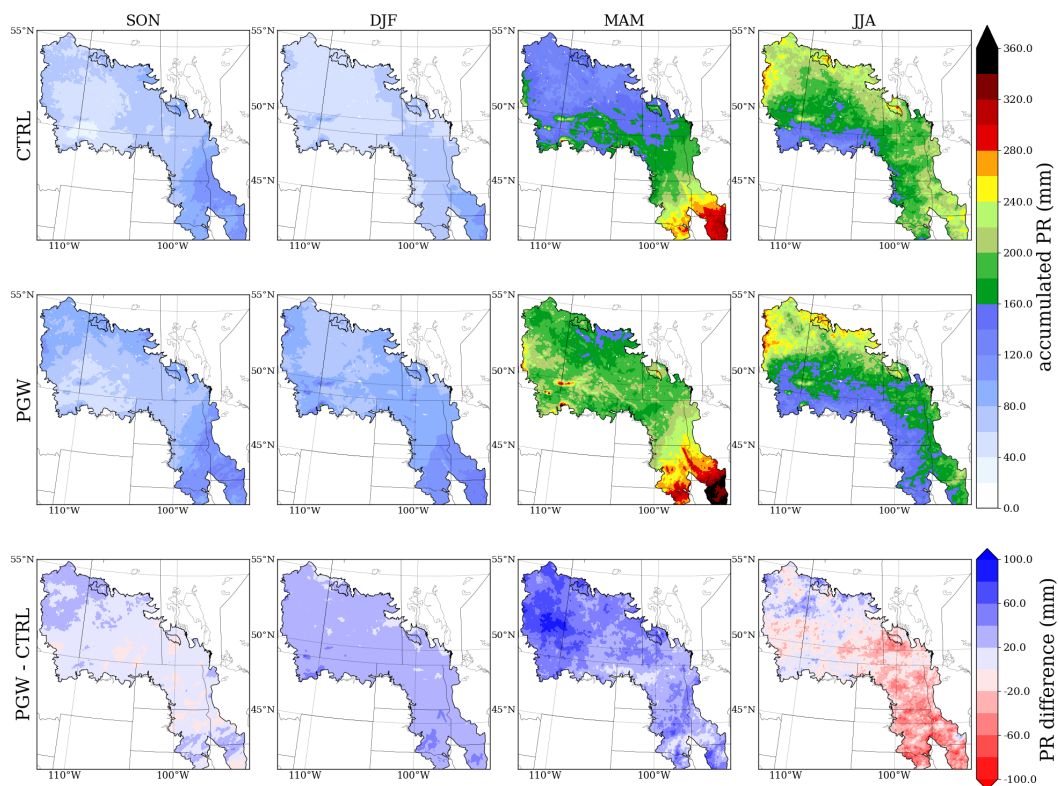
739

740

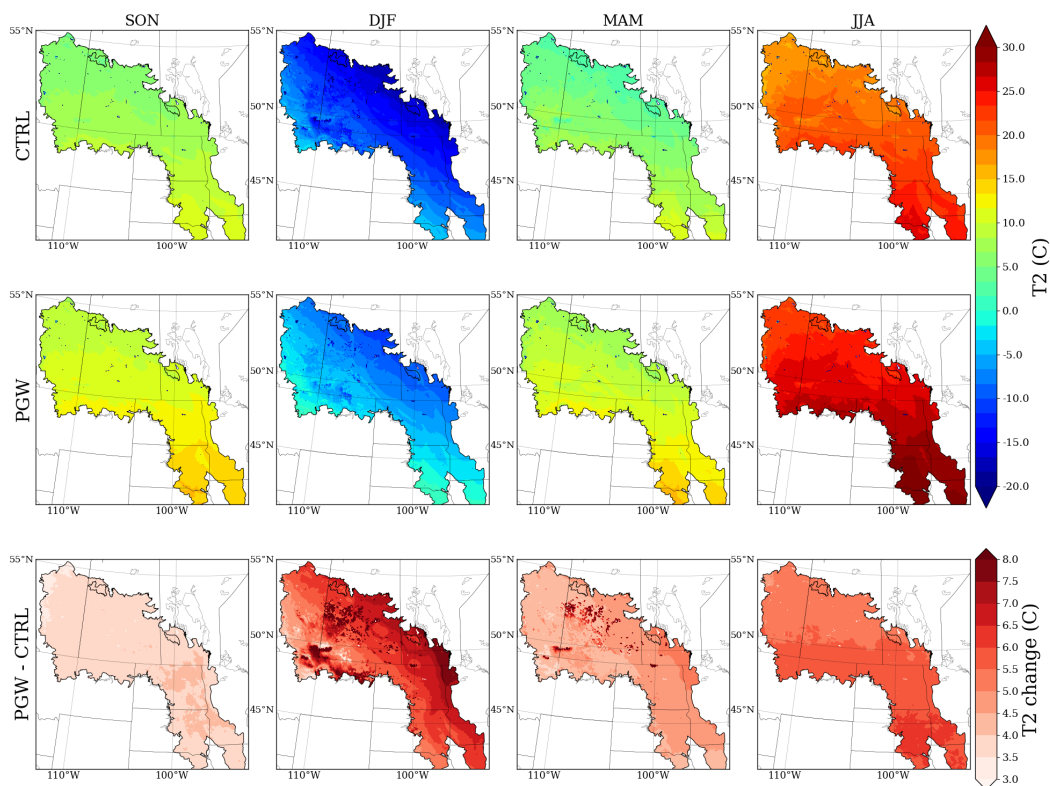
741

742

Fig. 3 Evaluation of the annual precipitation from two model products (b, f), WRF CONUS and NARR against rain gauge observation (a, e), their bias (c, g) and percentage bias (d, h).



743
744 **Fig. 4** Seasonal Accumulated precipitation from current climate (CTRL, top), future climate (PGW, middle) and
745 projected change (PGW-CTRL, bottom) in forcing data.
746

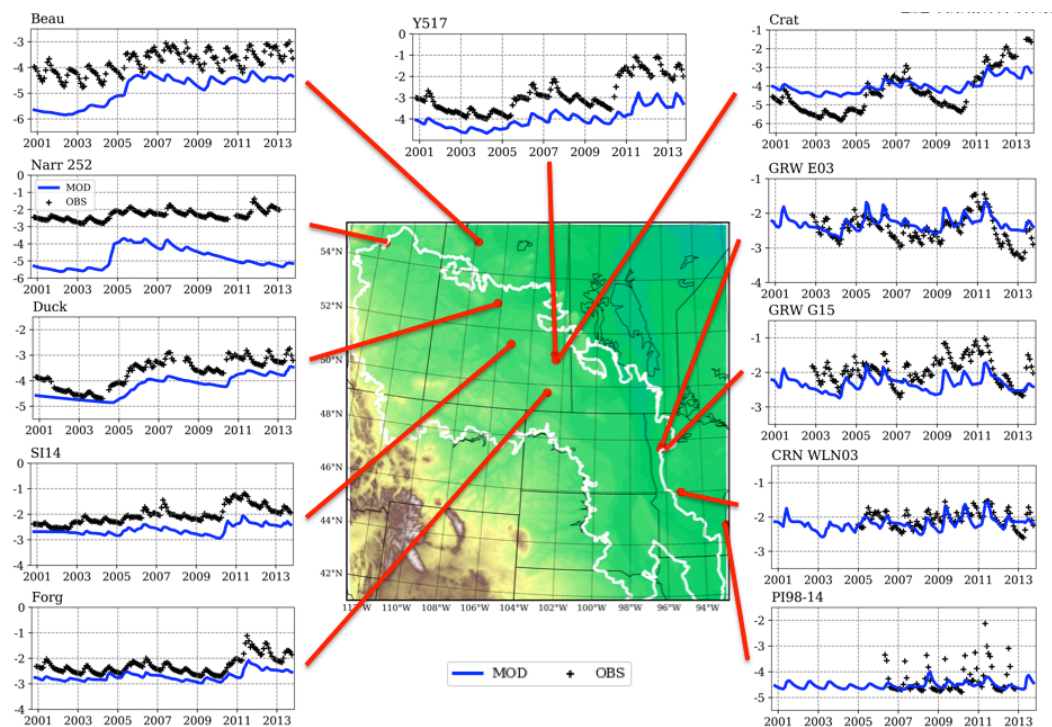


747
748
749
750

Fig. 5 Seasonal temperatures from current climate (CTRL, top), future climate (PGW, middle) and projected change (PGW-CTRL, bottom) in forcing data.

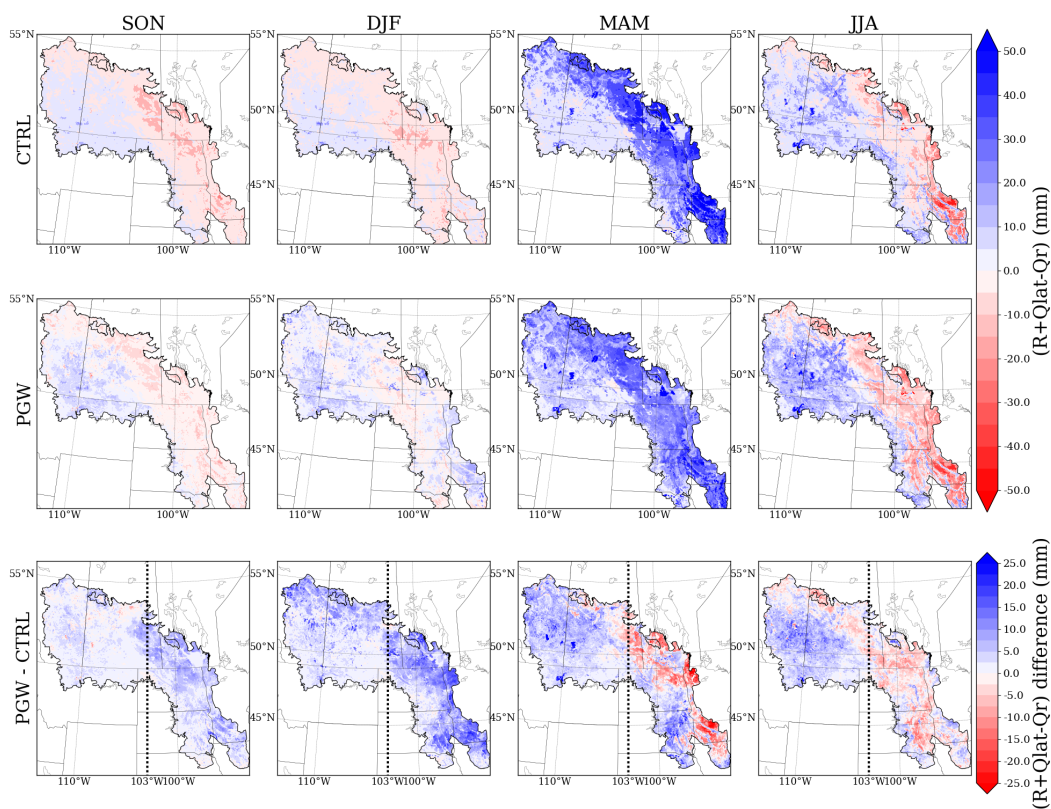


751



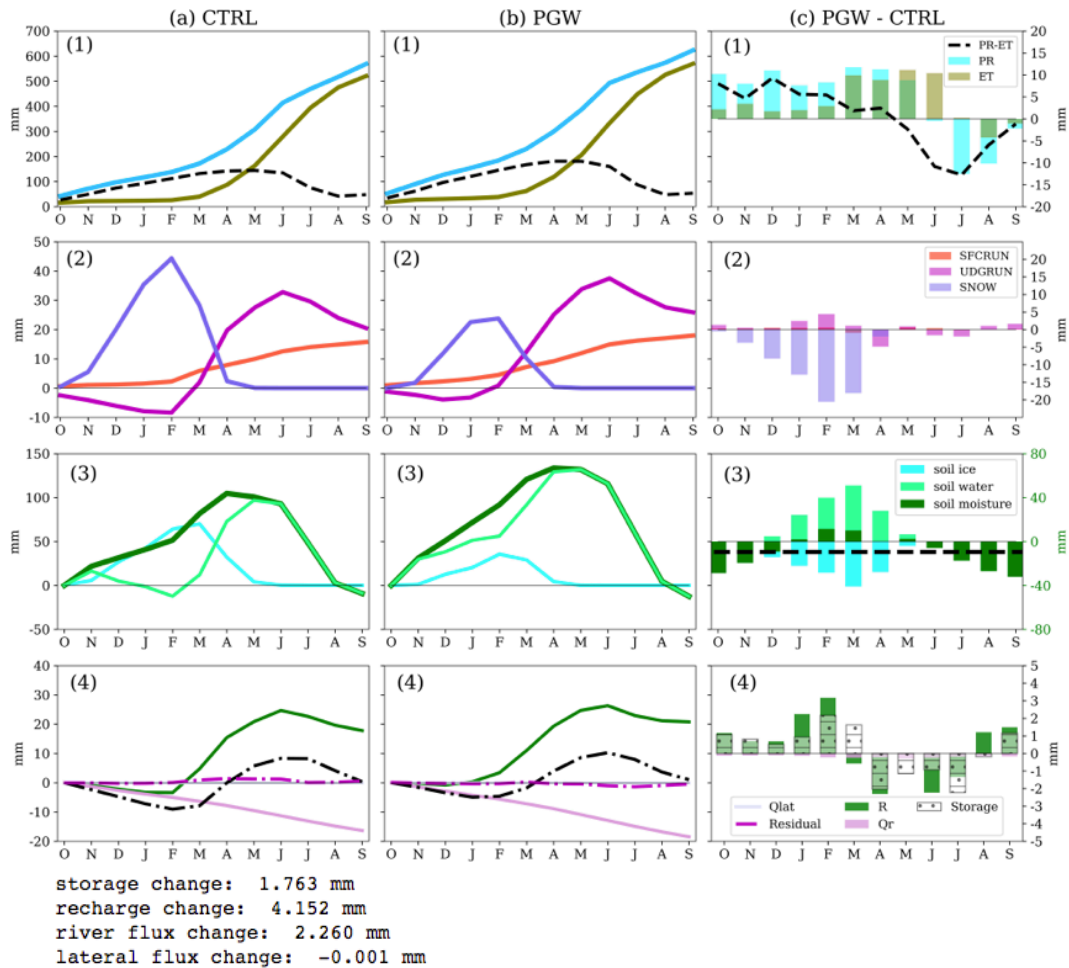
752
753
754

Fig. 6 WTD (m) from 11 groundwater wells and the model simulation results in PPR.



755
 756
 757
 758
 759

Fig. 7 Seasonal accumulated total groundwater fluxes ($R+Q_{lat}+Q_r$) for current climate (CTRL, top), future climate (PGW, middle) and projected change (PGW-CTRL, bottom) in forcing data. Black dashed lines in PGW-CTRL separate the PPR into eastern and western halves.



760

761

762

763

764

765

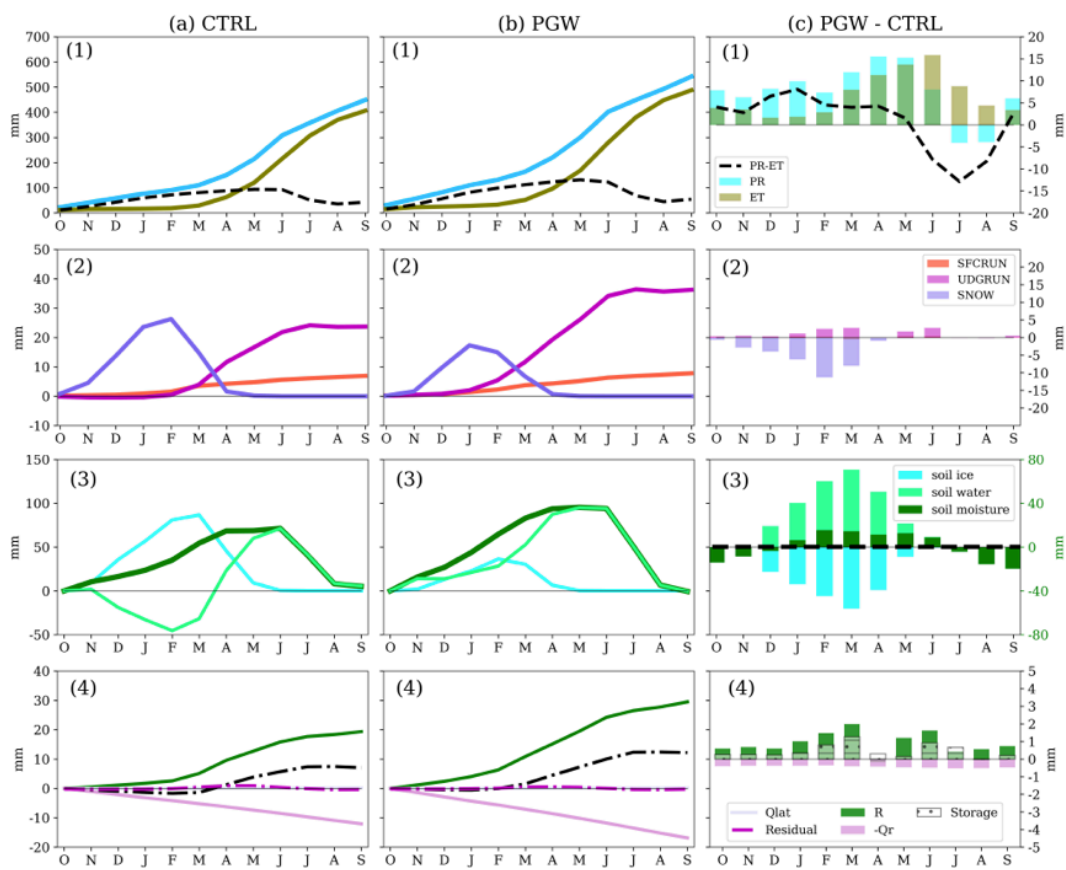
766

767

768

769

Fig. 8 Water budget analysis in the eastern PPR in (a) CTRL, (b) PGW and (c) PGW – CTRL. Water budget terms include: (1) *PR* & *ET*, (2) surface snow, surface runoff and underground runoff (*SNOW*, *SFCRUN*, and *UDGRUN*), (3) change of soil moisture storage (soil water, soil ice and total soil moisture, ΔSMC) and (4) groundwater fluxes and the change of groundwater storage (*R*, Q_{lat} , Q_r , ΔS_g). The annual mean soil moisture change (PGW-CTRL) is shown with black dashed line in (3). The Residual term is defined as $Res = (R + Q_{lat} - Q_r) - \Delta S_g$ in (4). Note that in (a) and (b) the accumulated fluxes and change in storage are shown in lines, whereas in (c) the difference in (PGW-CTRL) is shown for each individual month in bars.



storage change: 5.390 mm
 recharge change: 10.727 mm
 river flux change: 5.207 mm
 lateral flux change: 0.000 mm

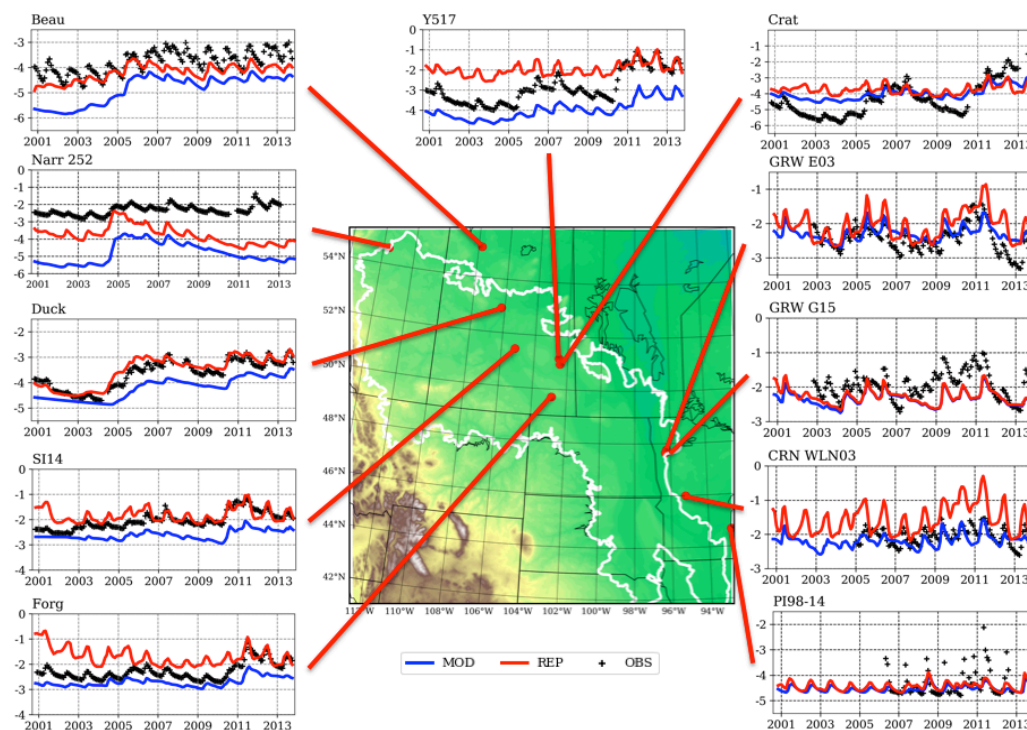
770

771

772

773

Fig. 9 Same as Fig. 8, but for the western PPR.



774
775
776
777
778
779

Fig. 10 Same as Fig. 6, the timeseries of simulated WTD from both default model (MOD) and replacing soil type simulation (REP). REP is the additional simulation by replacing the default soil type in the model with lithology type taken from observational surveys.